



# First observation and study of the $K^\pm \rightarrow \pi^\pm \pi^0 e^+ e^-$ decay

The NA48/2 Collaboration

J.R. Batley, G. Kalmus, C. Lazzeroni<sup>1,2</sup>, D.J. Munday<sup>1</sup>, M.W. Slater<sup>1</sup>, S.A. Wotton<sup>1</sup>

*Cavendish Laboratory, University of Cambridge, Cambridge, CB3 0HE, UK<sup>3</sup>*

R. Arcidiacono<sup>4</sup>, G. Bocquet, N. Cabibbo<sup>†</sup>, A. Ceccucci, D. Cundy<sup>5</sup>, V. Falaleev<sup>6</sup>,  
M. Fidecaro, L. Gatignon, A. Gonidec, W. Kubischta, A. Maier, A. Norton<sup>7</sup>, M. Patel<sup>8</sup>,  
A. Peters

*CERN, CH-1211 Genève 23, Switzerland*

S. Balev<sup>†</sup>, P.L. Frabetti, E. Gersabeck<sup>9</sup>, E. Goudzovski<sup>1,2,10</sup>, P. Hristov<sup>11</sup>, V. Kekelidze,  
V. Kozhuharov<sup>12,13</sup>, L. Litov<sup>12</sup>, D. Madigozhin, M. Misheva<sup>\*,14</sup>, N. Molokanova,  
I. Polenkevich, Yu. Potrebenikov, S. Stoynev<sup>15</sup>, A. Zinchenko<sup>†</sup>

*Joint Institute for Nuclear Research, 141980 Dubna (MO), Russia*

E. Monnier<sup>16</sup>, E. Swallow<sup>†</sup>, R. Winston<sup>17</sup>

*The Enrico Fermi Institute, The University of Chicago, Chicago, IL 60126, USA*

P. Rubin<sup>18</sup>, A. Walker

*Department of Physics and Astronomy, University of Edinburgh, Edinburgh, EH9 3JZ, UK*

P. Dalpiaz, C. Damiani, M. Fiorini, M. Martini, F. Petrucci, M. Savrié, M. Scarpa, H. Wahl

*Dipartimento di Fisica e Scienze della Terra dell'Università e Sezione dell'INFN di Ferrara, I-44122 Ferrara, Italy*

W. Baldini, A. Cotta Ramusino, A. Gianoli

*Sezione dell'INFN di Ferrara, I-44122 Ferrara, Italy*

M. Calvetti, E. Celeghini, E. Iacopini, M. Lenti, G. Ruggiero<sup>19</sup>

*Dipartimento di Fisica dell'Università e Sezione dell'INFN di Firenze, I-50125 Sesto Fiorentino, Italy*

A. Bizzeti<sup>20</sup>, M. Veltri<sup>21</sup>

*Sezione dell'INFN di Firenze, I-50019 Sesto Fiorentino, Italy*

M. Behler, K. Eppard, M. Hita-Hochgesand, K. Kleinknecht, P. Marouelli, L. Masetti,  
U. Moosbrugger, C. Morales Morales, B. Renk, M. Wache, R. Wanke, A. Winhart<sup>1</sup>

*Institut für Physik, Universität Mainz, D-55099 Mainz, Germany<sup>22</sup>*

D. Coward<sup>23</sup>, A. Dabrowski<sup>11</sup>, T. Fonseca Martin, M. Shieh, M. Szleper<sup>24</sup>, M. Velasco, M.D. Wood<sup>23</sup>

Department of Physics and Astronomy, Northwestern University, Evanston, IL 60208, USA

G. Anzivino, E. Imbergamo, A. Nappi<sup>†</sup>, M. Piccini, M. Raggi<sup>25</sup>, M. Valdata-Nappi

Dipartimento di Fisica dell'Università e Sezione dell'INFN di Perugia, I-06100 Perugia, Italy

P. Cenci, M. Pepe, M.C. Petrucci

Sezione dell'INFN di Perugia, I-06100 Perugia, Italy

F. Costantini, N. Doble, L. Fiorini<sup>26</sup>, S. Giudici, G. Pierazzini<sup>†</sup>, M. Sozzi, S. Venditti

Dipartimento di Fisica dell'Università e Sezione dell'INFN di Pisa, I-56100 Pisa, Italy

G. Collazuol<sup>27</sup>, L. DiLella<sup>28</sup>, G. Lamanna<sup>28</sup>, I. Mannelli, A. Michetti

Scuola Normale Superiore e Sezione dell'INFN di Pisa, I-56100 Pisa, Italy

C. Cerri, R. Fantechi

Sezione dell'INFN di Pisa, I-56100 Pisa, Italy

B. Bloch-Devaux<sup>\*,29</sup>, C. Cheshkov<sup>30</sup>, J.B. Chèze, M. De Beer, J. Derré, G. Marel, E. Mazzucato, B. Peyaud, B. Vallage

DSM/IRFU – CEA Saclay, F-91191 Gif-sur-Yvette, France

M. Holder, M. Ziolkowski

Fachbereich Physik, Universität Siegen, D-57068 Siegen, Germany<sup>31</sup>

S. Bifani<sup>1</sup>, M. Clemencic<sup>11</sup>, S. Goy Lopez<sup>32</sup>

Dipartimento di Fisica dell'Università e Sezione dell'INFN di Torino, I-10125 Torino, Italy

C. Biino, N. Cartiglia, F. Marchetto

Sezione dell'INFN di Torino, I-10125 Torino, Italy

H. Dibon, M. Jeitler, M. Markytan, I. Mikulec, G. Neuhofer, L. Widhalm<sup>†</sup>

Österreichische Akademie der Wissenschaften, Institut für Hochenergiephysik, A-10560 Wien, Austria<sup>33</sup>

## ARTICLE INFO

### Article history:

Received 11 September 2018  
Received in revised form 23 November 2018  
Accepted 26 November 2018  
Available online 29 November 2018  
Editor: W.-D. Schlatter

## ABSTRACT

The NA48/2 experiment at CERN reports the first observation of the  $K^\pm \rightarrow \pi^\pm \pi^0 e^+ e^-$  decay from an exposure of  $1.7 \times 10^{11}$  charged kaon decays recorded in 2003–2004. A sample of 4919 candidates with 4.9% background contamination allows the determination of the branching ratio in the full kinematic region,  $BR(K^\pm \rightarrow \pi^\pm \pi^0 e^+ e^-) = (4.24 \pm 0.14) \times 10^{-6}$ . The study of the kinematic space shows evidence for a structure dependent contribution in agreement with predictions based on chiral perturbation theory. Several P- and CP-violating asymmetries are also evaluated.

© 2018 The Author(s). Published by Elsevier B.V. This is an open access article under the CC BY license (<http://creativecommons.org/licenses/by/4.0/>). Funded by SCOAP<sup>3</sup>.

\* Corresponding authors.

E-mail addresses: [milena.misheva@cern.ch](mailto:milena.misheva@cern.ch) (M. Misheva), [brigitte.bloch-devaux@cern.ch](mailto:brigitte.bloch-devaux@cern.ch) (B. Bloch-Devaux).

† Deceased.

<sup>1</sup> Now at: School of Physics and Astronomy, University of Birmingham, Birmingham, B15 2TT, UK.

<sup>2</sup> Supported by a Royal Society University Research Fellowship (UF100308, UF0758946).

<sup>3</sup> Funded by the UK Particle Physics and Astronomy Research Council, grant PPA/G/O/1999/00559.

<sup>4</sup> Now at: Università degli Studi del Piemonte Orientale e Sezione dell'INFN di Torino, I-10125 Torino, Italy.

<sup>5</sup> Now at: Istituto di Cosmogeofisica del CNR di Torino, I-10133 Torino, Italy.

## 1. Introduction and theoretical framework

Kaon decays have played a major role in establishing the quark mixing flavour structure of the Standard Model [1]. Radiative kaon decays are of particular interest in testing models describing low-energy quantum chromodynamics (QCD) such as the chiral perturbation theory (ChPT), an effective field theory valid below a scale  $\mathcal{O}(1 \text{ GeV})$ .

The radiative decay  $K^\pm \rightarrow \pi^\pm \pi^0 e^+ e^-$ , never observed so far, proceeds through virtual photon exchange followed by internal conversion into an electron-positron pair, i.e.  $K^\pm \rightarrow \pi^\pm \pi^0 \gamma^* \rightarrow \pi^\pm \pi^0 e^+ e^-$ . The virtual  $\gamma^*$  can be produced by two different mechanisms: Inner Bremsstrahlung (IB) where the  $\gamma^*$  is emitted by one of the charged mesons in the initial or final state, and Direct Emission (DE) where the  $\gamma^*$  is radiated off at the weak vertex. Consequently, the differential decay rate consists of three terms: the dominant long-distance IB contribution, the DE component (electric E and magnetic M parts), and their interference. The interference term INT includes the different contributions, IB-E, IB-M and E-M. The IB-M and E-M terms are P-violating and cancel upon angular integration in the total rate.

There are few theoretical publications related to the  $K^\pm \rightarrow \pi^\pm \pi^0 e^+ e^-$  mode [2–4] and no experimental observation. The authors of [3] predicted, on the basis of the NA48/2 measurement of

the magnetic and electric terms involved in the  $K^\pm \rightarrow \pi^\pm \pi^0 \gamma$  decay [5], the branching ratios of IB, DE and INT components of the  $K^\pm \rightarrow \pi^\pm \pi^0 e^+ e^-$  decay and posted recently a revised work [6] where the interference term is re-evaluated using more realistic inputs based on additional experimental results and fewer theoretical assumptions.

It is worth writing explicitly the various contributions to the squared amplitude of the decay [3]:

$$\sum_{\text{spins}} |M|^2 = \frac{2e^2}{q^4} \left[ \sum_{i=1}^3 |F_i|^2 T_{ii} + 2 \text{Re} \sum_{i < j}^3 (F_i^* F_j) T_{ij} \right], \quad (1)$$

where  $F_i$  are complex form factors and  $T_{ij}$  are kinematic expressions (as defined in [3]) which depend on the four-momenta of the  $e^+ e^-$  system and the charged and neutral pions in the kaon rest frame. For convenience, one also writes:

$$F_1 = F_1^{IB} + F_1^{DE}, \quad F_2 = F_2^{IB} + F_2^{DE}, \quad F_3 = F_3^{DE}. \quad (2)$$

The form factors  $F_1^{IB}, F_2^{IB}$  include a strong phase  $\delta_0^2$  corresponding to the S-wave and isospin 2 state of the dipion system. The complex form factors  $F_1^{DE}, F_2^{DE}$  correspond to the electric part of DE and make use of the ChPT counterterms  $N_E^{(0,1,2)}$  while  $F_3^{DE}$  corresponds to the magnetic part of DE and makes use of the counterterm  $N_M^{(0)}$ . These form factors carry a strong phase  $\delta_1^1$  corresponding to the P-wave and isospin 1 state of the dipion system.

Numerical values of the counterterms were estimated [6] using experimental measurements of form factors in the related modes  $K^\pm \rightarrow \pi^\pm \gamma^*$ ,  $K_S \rightarrow \pi^0 \gamma^*$  and  $K^\pm \rightarrow \pi^\pm \pi^0 \gamma$ .

## 2. Kaon beam line and detector

The NA48/2 experiment at the CERN SPS was specifically designed for charge asymmetry measurements in the  $K^\pm \rightarrow 3\pi$  decay modes [7]. Large samples of charged kaon decays were collected during the 2003–2004 data taking period. The experiment beam line was designed to deliver simultaneous narrow momentum band  $K^+$  and  $K^-$  beams originating from primary 400 GeV/c protons extracted from the CERN SPS and impinging on a beryllium target. Secondary unseparated hadron beams with central momenta of 60 GeV/c and a momentum band of  $\pm 3.8\%$  (rms) were selected and brought to a common beam axis by two systems of dipole magnets with zero total deflection (called “achromats”), focusing quadrupoles, muons sweepers and collimators. The fraction of beam kaons decaying in the 114 m long cylindrical evacuated tank was 22%.

The momenta of charged decay products were measured in a magnetic spectrometer, housed in a tank filled with helium at nearly atmospheric pressure. The spectrometer was composed of pairs of drift chambers (DCH) on each side of a dipole magnet providing a momentum kick  $\Delta p = 120 \text{ MeV/c}$  to charged particles in the horizontal plane. The momentum resolution achieved was  $\sigma_p/p = (1.02 \oplus 0.044 \cdot p)\%$  ( $p$  in GeV/c).

A hodoscope (HOD) consisting of two planes of plastic scintillators, each segmented into 64 strip-shaped counters, followed the spectrometer and provided time measurements for charged particles with a resolution of 150 ps. Grouping the counters of each plane in eight subsets, the HOD surface was logically subdivided into 16 exclusive regions producing fast signals used to trigger the detector readout on charged track topologies.

Further downstream was a liquid krypton electromagnetic calorimeter (LKr), an almost homogeneous ionization chamber with an active volume of  $7 \text{ m}^3$ , segmented transversally into 13248 projective  $2 \times 2 \text{ cm}^2$  cells with no longitudinal segmentation. The energies of photons and electrons were measured with

<sup>6</sup> Now at: Joint Institute for Nuclear Research, 141980 Dubna (MO), Russia.

<sup>7</sup> Now at: Dipartimento di Fisica e Scienze della Terra dell'Università e Sezione dell'INFN di Ferrara, I-44122 Ferrara, Italy.

<sup>8</sup> Now at: Department of Physics, Imperial College, London, SW7 2BW, UK.

<sup>9</sup> Now at: School of Physics and Astronomy, The University of Manchester, Manchester, M13 9PL, UK.

<sup>10</sup> Supported by ERC Starting Grant 336581.

<sup>11</sup> Now at: CERN, CH-1211 Genève 23, Switzerland.

<sup>12</sup> Now at: Faculty of Physics, University of Sofia “St. Kl. Ohridski”, BG-1164 Sofia, Bulgaria, funded by the Bulgarian National Science Fund under contract DID02-22.

<sup>13</sup> Also at: Laboratori Nazionali di Frascati, I-00044 Frascati, Italy.

<sup>14</sup> Now at: Institute of Nuclear Research and Nuclear Energy of Bulgarian Academy of Science (INRNE-BAS), BG-1784 Sofia, Bulgaria.

<sup>15</sup> Now at: Fermi National Accelerator Laboratory, Batavia, IL 60510, USA.

<sup>16</sup> Now at: Centre de Physique des Particules de Marseille, IN2P3-CNRS, Université de la Méditerranée, F-13288 Marseille, France.

<sup>17</sup> Now at: School of Natural Sciences, University of California, Merced, CA 95343, USA.

<sup>18</sup> Now at: School of Physics, Astronomy and Computational Sciences, George Mason University, Fairfax, VA 22030, USA.

<sup>19</sup> Now at: Physics Department, University of Lancaster, Lancaster, LA1 4YW, UK.

<sup>20</sup> Also at Dipartimento di Scienze Fisiche, Informatiche e Matematiche, Università di Modena e Reggio Emilia, I-41125 Modena, Italy.

<sup>21</sup> Also at Istituto di Fisica, Università di Urbino, I-61029 Urbino, Italy.

<sup>22</sup> Funded by the German Federal Minister for Education and research under contract 05HK1UM1/1.

<sup>23</sup> Now at: SLAC, Stanford University, Menlo Park, CA 94025, USA.

<sup>24</sup> Now at: National Center for Nuclear Research, P-05-400 Świerk, Poland.

<sup>25</sup> Now at: Università di Roma “La Sapienza”, I-00185 Roma, Italy.

<sup>26</sup> Now at: Instituto de Física Corpuscular IFIC, Universitat de València, E-46071 València, Spain.

<sup>27</sup> Now at: Dipartimento di Fisica dell'Università e Sezione dell'INFN di Padova, I-35131 Padova, Italy.

<sup>28</sup> Now at: Dipartimento di Fisica dell'Università e Sezione dell'INFN di Pisa, I-56100 Pisa, Italy.

<sup>29</sup> Now at: Dipartimento di Fisica dell'Università di Torino, I-10125 Torino, Italy.

<sup>30</sup> Now at: Institut de Physique Nucléaire de Lyon, IN2P3-CNRS, Université Lyon I, F-69622 Villeurbanne, France.

<sup>31</sup> Funded by the German Federal Minister for Research and Technology (BMBF) under contract 056SI74.

<sup>32</sup> Now at: Centro de Investigaciones Energeticas Medioambientales y Tecnológicas, E-28040 Madrid, Spain.

<sup>33</sup> Funded by the Austrian Ministry for Traffic and Research under the contract GZ 616.360/2-IV GZ 616.363/2-VIII, and by the Fonds für Wissenschaft und Forschung WWF Nr. P08929-PHY.

resolutions  $\sigma_E/E = (3.2/\sqrt{E} \oplus 9.0/E \oplus 0.42)\%$ . The transverse positions of isolated showers were measured with a spatial resolution  $\sigma_x = \sigma_y = (0.42/\sqrt{E} \oplus 0.06)$  cm, and the shower time resolution was  $2.5 \text{ ns}/\sqrt{E}$  ( $E$  in GeV). An iron/scintillator hadronic calorimeter and muon detectors were located further downstream. Neither of them was used in the present analysis.

A dedicated two-level trigger was used to collect  $K^\pm$  decays into three charged tracks with high efficiency: at the first level (L1), events containing charged tracks were selected by requiring space and time coincidences of signals in the two HOD planes in at least two of the 16 exclusive regions; at the second level (L2), a farm of asynchronous microprocessors performed a fast track reconstruction and ran a vertex finding algorithm.

More details about the beam line and trigger implementation can be found in [7]. A detailed description of the detector can be found in [8].

### 3. Data analysis

#### 3.1. Measurement method

The  $K^\pm \rightarrow \pi^\pm \pi^0 e^+ e^-$  decay rate is measured relative to the normalization decay  $K^\pm \rightarrow \pi^\pm \pi^0$  collected concurrently with the same trigger logic. This method does not rely on an absolute kaon flux measurement. In the signal sample, the  $\pi^0$  is identified through the  $\pi^0 \rightarrow \gamma\gamma$  mode ( $\pi_{\gamma\gamma}^0$ ). In the normalization sample, the  $\pi^0$  is identified through the  $\pi_D^0 \rightarrow e^+ e^- \gamma$  Dalitz mode ( $\pi_D^0$ ). The ratio of partial rates (and branching ratios) is obtained as:

$$\begin{aligned} BR(K^\pm \rightarrow \pi^\pm \pi^0 e^+ e^-) / BR(K^\pm \rightarrow \pi^\pm \pi^0) \\ = \frac{N_s - N_{bs}}{N_n - N_{bn}} \cdot \frac{A_n \times \varepsilon_n}{A_s \times \varepsilon_s} \cdot \frac{\Gamma(\pi_D^0)}{\Gamma(\pi_{\gamma\gamma}^0)}, \end{aligned} \quad (3)$$

where  $N_s, N_n$  are the numbers of signal and normalization candidates;  $N_{bs}, N_{bn}$  are the numbers of background events in the signal and normalization samples;  $A_s$  and  $\varepsilon_s$  are the acceptance and the trigger efficiency for the signal sample;  $A_n$  and  $\varepsilon_n$  are those for the normalization sample.

The branching ratio of the normalization mode is  $BR(K^\pm \rightarrow \pi^\pm \pi^0) = (20.67 \pm 0.08)\%$  and the ratio of  $\pi^0$  partial rates is  $\Gamma(\pi_D^0)/\Gamma(\pi_{\gamma\gamma}^0) = (1.188 \pm 0.035)\%$  [9]. Acceptances are obtained from a detailed Monte Carlo (MC) simulation based on GEANT3 [10]. The simulation includes full detector geometry and material description, stray magnetic fields, DCH local inefficiencies and misalignment, LKr local inefficiencies, accurate simulation of the kaon beam line and variations of the above throughout the data-taking period.

Efficiencies of the L1 and L2 triggers are measured from down-scaled control samples, recorded concurrently with the three-track trigger. The control trigger condition for the L1 efficiency measurement requires at least one coincidence of signals in the two planes of the HOD. The control trigger sample for the L2 efficiency measurement consists of L1 triggers recorded regardless of the L2 decision. The trigger decision is also available in the simulation for comparison.

#### 3.2. Event reconstruction and selection

The standard NA48/2 software has been used including charged track, LKr energy cluster and three-track decay vertex reconstruction [7]. Fully reconstructed  $K^\pm \rightarrow \pi^\pm \pi^+ \pi^-$  decays have been used to monitor the DCH alignment, the spectrometer field integral and the mean beam position at each DCH plane throughout the data taking.

Signal and normalization candidates are reconstructed from three tracks: two same-sign tracks and one opposite-charge track forming a common vertex in the fiducial decay volume, the vertex charge being therefore  $q_{vtx} = \pm 1$ . The vertex time is defined as the average of the three HOD signal times associated to the tracks. The tracks are required to be in time within 5 ns of the vertex time. Their impact points are required to be within the geometrical acceptance of the drift chambers. In particular, the track distance to the monitored beam position in DCH1 plane is required to be larger than 12 cm. The track momenta are required to be in the range (2–60) GeV/c and track-to-track distances at DCH1 to be larger than 2 cm to suppress photon conversions to  $e^+ e^-$  pairs in the upstream material.

Configurations where the three considered tracks, extrapolated to the HOD front face, have their impact points in a single trigger region are rejected to avoid L1 inefficiencies of purely geometrical origin. Because of the different kinematics, this affects 2.3% of the signal sample and has a negligible effect on the normalization sample.

All vertices considered for further analysis are required to be reconstructed in a 98 m long fiducial volume, starting 2 m downstream of the last collimator exit, and within 3 cm from the beam axis.

Photon clusters matching the vertex time within 5 ns are considered as photon candidates if their energy is in the range (3–60) GeV, their position is within the LKr geometrical acceptance and their distance to the nearest LKr inactive cell is larger than 2 cm. Photon four-momenta are reconstructed assuming they originate from the three-track vertex. Photon trajectories are required to intercept the DCH1 plane at a radial position larger than 11 cm to avoid possible interactions with the DCH flange resulting in a degraded energy measurement.

Signal and normalization modes differ in their final state by one photon, while satisfying similar kinematic constraints on the reconstructed  $\pi^0$  and kaon masses, although with different resolutions because of different numbers of participating particles. The mass resolutions (Gaussian rms) obtained from the data agree with those from simulation and are found to be  $\sigma_m(\pi_D^0) \simeq 1.7 \text{ MeV}/c^2$ ,  $\sigma_m(\pi^\pm \pi_D^0) \simeq 4.2 \text{ MeV}/c^2$  and  $\sigma_m(\pi_{\gamma\gamma}^0) \simeq 2.7 \text{ MeV}/c^2$ ,  $\sigma_m(\pi^\pm \pi_{\gamma\gamma}^0 ee) \simeq 6.1 \text{ MeV}/c^2$  for the normalization and signal modes, respectively.

Very loose requirements are applied to the reconstructed masses, required to be within  $15 \text{ MeV}/c^2$  ( $45 \text{ MeV}/c^2$ ) from the nominal  $\pi^0$  ( $K^\pm$ ) mass [9], respectively, ensuring a minimal dependence of the selection on momentum or energy calibration effects, as well as on any resolution mismatches between data and simulation. A common constraint, taking into account the correlation between the reconstructed  $m_{\pi^0}$  and  $m_K$  masses and defined as

$$|m_{\pi^0} - 0.42 \cdot m_K + 72.3| < 6 \text{ (all masses in MeV}/c^2\text{)}, \quad (4)$$

contains more than 99% of the normalization events and about 96.5% of the signal events.

In both modes, the single track with its charge opposite to  $q_{vtx}$  is considered to be an electron (positron). The remaining  $e/\pi$  ambiguity for the two same-sign tracks is then solved by testing the two mass hypotheses against the full selection. When a particular mass assignment is considered, an extra requirement on the distance of any photon cluster to the track impact at the LKr front face is applied to guarantee photon shower isolation, avoiding potential overlap with other showers: the distance between the photon position and the electron and positron track impacts is required to be larger than 10 cm and the distance between the photon position and the pion track impact to be larger than 20 cm.



This requirement is enforced only for track impacts within the LKr geometrical acceptance.

No upper limit on the number of tracks and clusters is set, all three-track vertices being considered and combined with any photon cluster under the two possible  $e/\pi$  mass hypotheses until one combination satisfies either of the following selections (normalization or signal) below, the event being rejected otherwise. If both mass combinations are accepted, the one with the tighter constraint of Eq. (4) is kept.

**Normalization selection** The  $\pi_D^0$  candidate is reconstructed from a pair of electron and positron tracks and a photon originating from the three-track vertex. The kaon candidate is reconstructed from the  $\pi^\pm\pi_D^0$  system.

The consistency of the final state with a kaon decay along the beam axis is checked further by considering the energy-weighted coordinates of the centre of gravity (COG) of the particles at the LKr front plane computed from the photon position and the track extrapolations obtained from track parameters measured before the magnet (undeviated trajectories). The radial distance of the COG to the nominal beam position is required to be smaller than 2 cm. The pion momentum is required to be larger than 10 GeV/c and the total momentum of the system to be in the beam momentum range (54–66) GeV/c. The  $e^+e^-$  mass is required to be larger than 10 MeV/c<sup>2</sup> to ensure good agreement between data and simulation. A sample of 16316690 candidates satisfies the normalization selection criteria.

**Signal selection** The  $\pi_{\gamma\gamma}^0$  candidate is reconstructed from two photons originating from the three-track vertex. The kaon candidate is reconstructed from the  $\pi^\pm\pi^0e^+e^-$  system. The two photon clusters are required to be separated by more than 10 cm at the LKr front plane to avoid shower overlap. The event COG coordinates are then obtained including the two photons and the three charged tracks, and subjected to the same requirement as above. The total momentum of the system is required to be in the beam momentum range (54–66) GeV/c. The  $e^+e^-$  mass is required to be larger than 3 MeV/c<sup>2</sup>.

Two main sources of background contribute to the signal final state:  $K^\pm \rightarrow \pi^\pm\pi_{\gamma\gamma}^0\pi_D^0$  ( $K_{3\pi D}$ ) where one of the photons is lost (or merged with another particle), and  $K^\pm \rightarrow \pi^\pm\pi_D^0(\gamma)$  ( $K_{2\pi D\gamma}$ ), where the radiative photon and the Dalitz decay photon mimic a  $\pi^0 \rightarrow \gamma\gamma$  decay. Suppression of the  $K_{3\pi D}$  background events is achieved by requiring the squared mass of the  $\pi^+\pi^0$  system to be greater than 0.12 (GeV/c<sup>2</sup>)<sup>2</sup>, exploiting the larger phase space available in the signal mode. This cut alone rejects 94% of the  $K_{3\pi D}$  simulated events and  $\sim 1\%$  of the IB signal. To reject the  $K_{2\pi D\gamma}$  background, each of the two possible masses  $m_{e\gamma}$  is required to be more than 7 MeV/c<sup>2</sup> away from the nominal  $\pi^0$  mass (corresponding to about  $4\sigma$  of the mass resolution). A sample of 4919 candidates satisfies the signal selection criteria.

### 3.3. Background evaluation

The background processes contributing to the normalization mode ( $K_{2\pi D}$ ) are semi-leptonic decays followed by a Dalitz decay of the  $\pi^0$ :  $K^\pm \rightarrow \mu^\pm\nu\pi_D^0$  ( $K_{\mu 3D}$ ) and  $K^\pm \rightarrow e^\pm\nu\pi_D^0$  ( $K_{e 3D}$ ), collectively denoted  $K_{l3D}$ , where the  $\pi_D^0$  decay is correctly reconstructed but the lepton ( $\mu^\pm, e^\pm$ ) is erroneously attributed the  $\pi^+$  mass. The acceptances of such processes in the normalization selection are  $\mathcal{O}(10^{-4})$  and obtained from large simulated samples.

For each background process, the number of events  $N_{bn}$  is estimated relative to the number of observed events in the normalization mode  $N_n$  using the acceptances in the normalization selection and the world average branching ratios [9]:

$$K_{l3D} : N_{bn}/N_n = (A_{K_{l3D}}/A_n) \cdot BR(K_{l3D})/BR(K_{2\pi D}) \quad (5)$$

where the trigger efficiencies cancel to first order due to the similar topologies.

The number of background events in the signal selection  $N_{bs}$  is estimated relative to the number of observed events in the normalization selection  $N_n$  and is obtained as in Eq. (5), using the acceptances in the signal selection, both  $\mathcal{O}(10^{-6})$ :

$$K_{3\pi D} : N_{bs}/N_n = 2 \times (A_{K_{3\pi D}}/A_n) \cdot BR(K_{3\pi D}) \times BR(\pi^0 \rightarrow \gamma\gamma)/BR(K_{2\pi D}), \quad (6)$$

$$K_{2\pi D\gamma} : N_{bs}/N_n = A_{K_{2\pi D\gamma}}/A_n. \quad (7)$$

Note the factor of two in Eq. (6) due to the two  $\pi^0$  mesons in the  $K_{3\pi D}$  mode. An order of magnitude smaller contribution from  $K_{e3D}$  is also considered. In all contributions both background and normalization branching ratios include the  $\pi^0$  Dalitz decay partial rate whose value and uncertainty cancel in the estimation.

## 4. Branching ratio measurement

**Candidates and background** Samples of  $16.3 \times 10^6 K_{2\pi D}$  candidates and 4919 signal candidates have been selected from a subset of a  $1.7 \times 10^{11}$  kaon decay exposure in 2003–2004. The background estimates from simulation amount to  $(10437 \pm 119) K_{\mu 3D}$  events and  $(6851 \pm 106) K_{e3D}$  events in the normalization mode, corresponding to a total relative background contribution of 0.11%. In the signal mode, they amount to  $(132 \pm 8)$  events from  $K_{3\pi D}$ ,  $(102 \pm 19)$  events from  $K_{2\pi D\gamma}$  and  $(7 \pm 3)$  from  $K_{e3D}$ , adding up to a relative background contribution of  $(4.9 \pm 0.4)\%$ . The reconstructed  $\gamma e^+e^-$  ( $\gamma\gamma$ ) and  $\pi^\pm\pi_D^0$  ( $\pi^\pm\pi^0e^+e^-$ ) mass distributions are displayed in Fig. 1 (Fig. 2) for the selected normalization (signal) candidates. Background and normalization (signal) simulations, scaled to the number of observed candidates, show a good agreement with the data distributions.

**Acceptances** Because the selection acceptance is not uniform across the phase space, its overall value depends on the dynamics of the considered process. The acceptance  $A_n$  (3.981%) is computed using the simulation of  $K^\pm \rightarrow \pi^\pm\pi^0$  according to [11] followed by  $\pi_D^0$  decay according to the most recent “Prague” radiative decay calculation [12].

The MC samples for the different  $K^\pm \rightarrow \pi^\pm\pi^0e^+e^-$  signal contributions IB, DE and INT have been generated separately according to the theoretical description given in [3,6]: the DE contribution consists mainly of the magnetic M term, with the E term expected to be fifteen times lower; the INT term includes only the electric interference IB-E, as the other interference terms IB-M and E-M do not contribute to the total rate in the limit of full angular integration (Section 1). Particular care has been taken in the generation of the IB-E term which contributes constructively or destructively to the differential rate depending on the kinematic space region considered. This property is illustrated in Fig. 3-left. Radiative effects are implemented using the PHOTOS package [13].

Global acceptances are obtained for each of the three main components of the signal process: IB ( $0.645 \pm 0.001\%$ ), M ( $1.723 \pm 0.003\%$ ) and IB-E ( $0.288 \pm 0.001\%$ ). The signal acceptance  $A_s$  is then obtained from a weighted average of the single-component acceptances, using as weights,  $w$ , their relative contributions to the total rate with respect to IB computed in [3,6]:

$$A_s = \frac{A_{IB} + A_M \cdot w_M + A_{IB-E} \cdot w_{IB-E}}{1 + w_M + w_{IB-E}}, \quad (8)$$

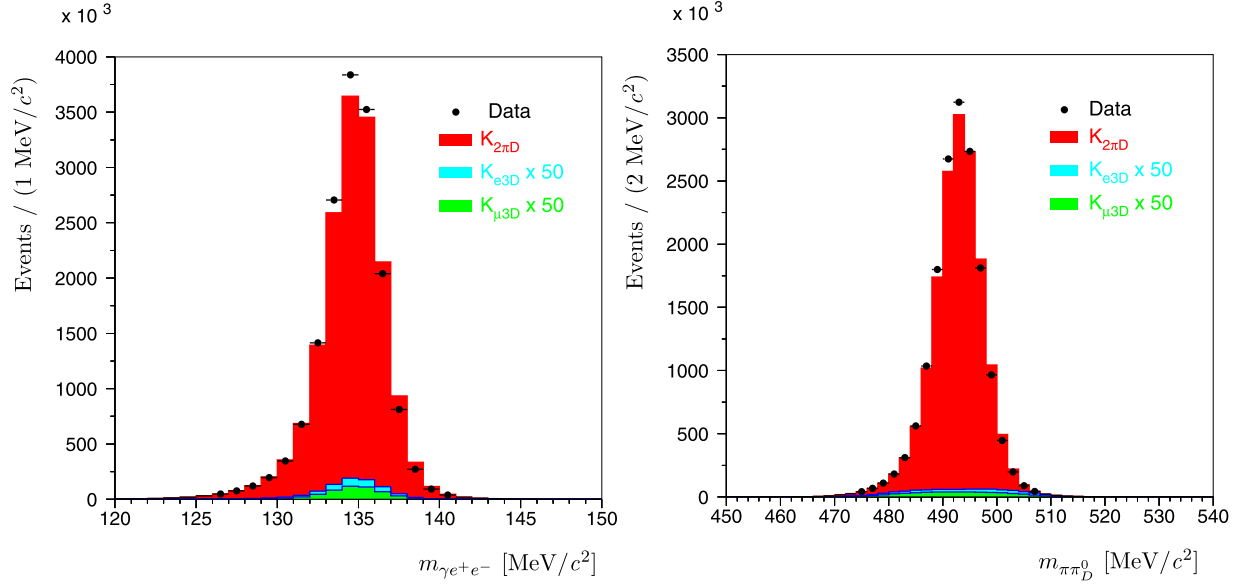


**Fig. 1.** Normalization candidates. Left: reconstructed  $\gamma e^+ e^-$  mass. Right: reconstructed  $\pi^+ \pi_D^0$  mass. Full dots correspond to data candidates; stacked histograms are, from bottom to top, the expected  $K_{\mu 3D}$  (green) and  $K_{e 3D}$  (blue) backgrounds multiplied by a factor of 50 to be visible. The normalization simulation (red) includes radiative effects in both kaon and  $\pi_D^0$  decays that reproduce the asymmetric tails of both distributions.

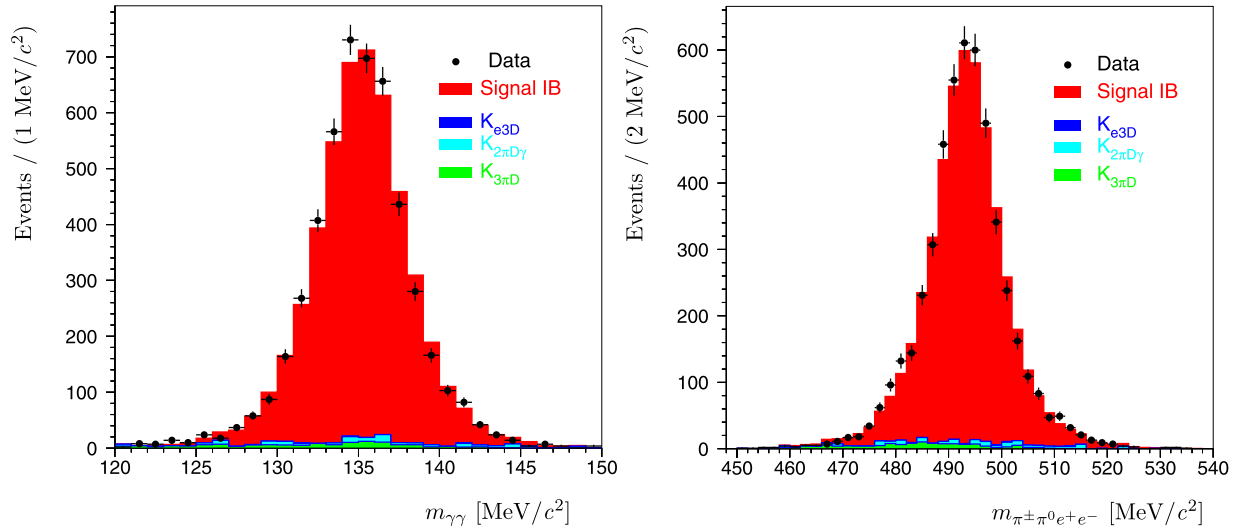


**Fig. 2.** Signal candidates. Left: reconstructed  $\gamma\gamma$  mass. Right: reconstructed  $\pi^+ \pi_D^0 e^+ e^-$  mass. Full dots correspond to data candidates; stacked histograms are, from bottom to top, the expected  $K_{3\pi D}$  (green),  $K_{2\pi D\gamma}$  (light blue) and  $K_{e 3D}$  (dark blue) backgrounds and IB signal (red) estimated from simulation. All quoted errors are statistical.

where  $w_M$  and  $w_{IB-E}$  are equal to  $1/71$  and  $-1/253$  respectively. The resulting signal acceptance is obtained as  $A_S = 0.9900 A_{IB} + 0.0139 A_M - 0.0039 A_{IB-E} = (0.662 \pm 0.001)\%$ .

Both normalization and signal acceptances are obtained with respect to the full  $m_{ee}$  kinematic range.

**Trigger efficiencies** Trigger efficiencies are measured from control data samples for the normalization mode (L1:  $(99.75 \pm 0.01)\%$ , L2:  $(97.66 \pm 0.04)\%$ ) and cross-checked against the simulated estimations (L1:  $(99.767 \pm 0.003)\%$ , L2:  $(98.495 \pm 0.006)\%$ ) which provide also an accurate description of their time variations due to local and temporary inefficiencies of the HOD or DCHs. Due to the low statistics of the signal candidate sample, it is not possible to obtain the trigger efficiencies from the downscaled control samples. Trigger efficiencies for the signal candidates are therefore estimated from the simulated samples (L1:  $(99.729 \pm 0.009)\%$ , L2:  $(98.604 \pm 0.021)\%$ ) and not affected by otherwise large statis-

tical uncertainties. The full trigger efficiency in each selection is obtained as the product of L1 and L2 efficiencies that are based on different detectors and therefore uncorrelated.

**Systematic uncertainties** The statistical uncertainties on acceptance and trigger efficiency values are accounted as part of the systematic uncertainties.

The control of the geometrical acceptances is evaluated by considering three exclusive regions of the decay longitudinal position (shown in Fig. 3-right) with different acceptances and background conditions for both signal and normalization channels. The difference between the statistical combination of the three  $BR$  values and the global value is quoted as systematic uncertainty.

The control of the acceptance dependence with time and kaon charge is quantified by considering four exclusive  $BR$  measurements (2003 and 2004 data sets,  $K^+$  and  $K^-$  decays) and quot-

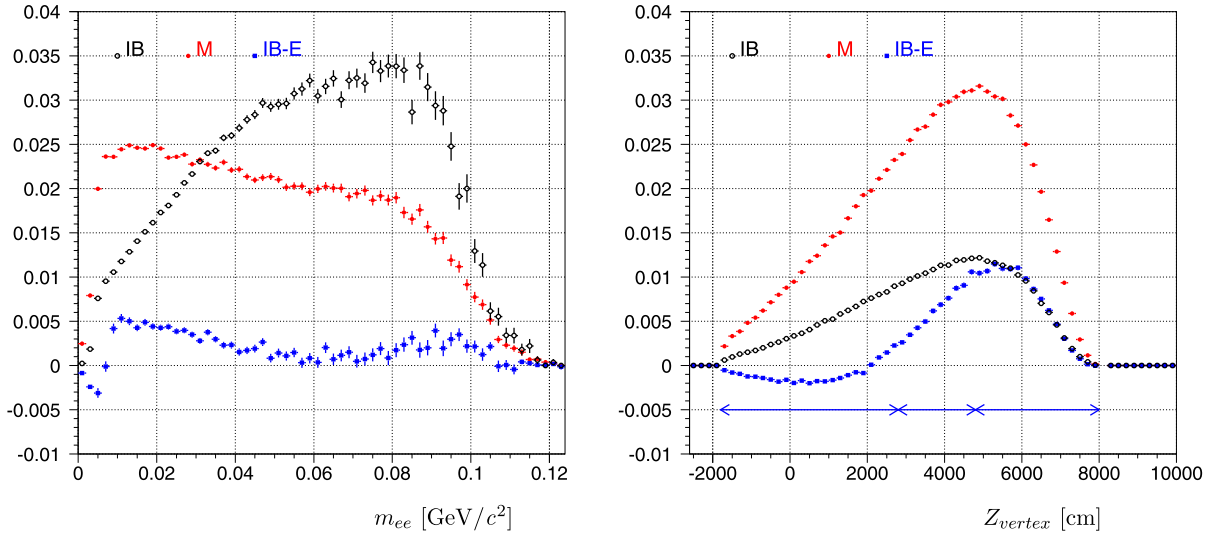


**Fig. 3.** Acceptances of the IB, M and IB-E components projected along the  $m_{ee}$  and the longitudinal vertex position  $Z_{vertex}$  variables (the Z axis origin is located 18 m downstream of the last collimator exit). For the IB-E component, the acceptance is formally plotted with a negative (positive) value when the interference is destructive (constructive). The arrows correspond to the three exclusive regions considered.

ing as systematic uncertainty the difference between the statistical combination of the four  $BR$  values and the global value.

An evaluation of the background control level is obtained by tightening the constraint of Eq. (4) to reduce the background to signal contribution from 4.9% to 3% while decreasing the signal acceptance by a relative fraction of 8%. The quoted uncertainty covers also the effect of the residual disagreement between data and simulated reconstructed masses.

Trigger efficiencies obtained from simulation are used in the  $BR$  calculation. The difference between the measured and simulated efficiencies of the normalization candidates is considered as a systematic uncertainty.

The model dependence of the signal acceptance is investigated by varying in turn each input ( $N_M^{(0)}$ ,  $N_E^{(0,1,2)}$ ) within its theoretical uncertainty estimate. The resulting variations in acceptance are added in quadrature to obtain the overall contribution to systematics.

According to the authors of the PHOTOS package [14], the uncertainty on the photon emission implementation cannot exceed 10% of the full effect (here  $4.9 \times 10^{-2}$  relative in the signal mode), which is quoted as systematic uncertainty. In the normalization mode, in the absence of any prescription from the authors of the “Prague”  $\pi_D^0$  decay implementation, 10% of the  $0.53 \times 10^{-2}$  relative difference between the PHOTOS and “Prague”  $K_{2\pi D}$  acceptances is conservatively assigned as a systematic uncertainty and added quadratically to the signal PHOTOS uncertainty. The agreement between data and simulation can be judged from the  $m_{ee}$  distributions of Fig. 4.

External errors stem from relative errors on  $BR(K^\pm \rightarrow \pi^\pm \pi^0)$  and on  $\Gamma(\pi_D^0)/\Gamma(\pi_{\gamma\gamma}^0)$ .

Table 1 summarizes the considered sources of uncertainty.

**Result** The final result is obtained as:

$$BR(K^\pm \rightarrow \pi^\pm \pi^0 e^+ e^-) = (4.237 \pm 0.063_{stat} \pm 0.033_{syst} \pm 0.126_{ext}) \times 10^{-6}, \quad (9)$$

where the statistical error is dominated by the signal statistics, the systematic error by the radiative effects and the external error by the  $\pi_D^0$  branching ratio uncertainty.

This value can be compared to the predictions from [3,6]:  $BR(K^\pm \rightarrow \pi^\pm \pi^0 e^+ e^-) = 4.183 \times 10^{-6}$  for IB only,  $BR(K^\pm \rightarrow$

**Table 1**

Statistical, systematic and external uncertainties to the  $K^\pm \rightarrow \pi^\pm \pi^0 e^+ e^-$  branching ratio measurement. The uncertainties related to the model dependence and to radiative effects can also be considered as external errors as being unrelated to our data.

Source	$\delta BR/BR \times 10^2$
$N_s$	1.426
$N_{bs}$	0.416
$N_n$	0.025
$N_{bn}$	negl.
Total statistical	1.486
$A_s$ (MC statistics)	0.171
$A_n$ (MC statistics)	0.051
$\varepsilon(L1_s \times L2_s)$ (MC statistics)	0.023
$\varepsilon(L1_n \times L2_n)$ (MC statistics)	0.007
Acceptance geometry control	0.083
Acceptance time variation control	0.064
Background control	0.280
Trigger efficiency (systematics)	0.400
Model dependence	0.285
Radiative effects	0.490
Total systematic	0.777
$BR(K_{2\pi})$	0.387
$\Gamma(\pi_D^0)/\Gamma(\pi_{\gamma\gamma}^0)$	2.946
Total external	2.971

$\pi^\pm \pi^0 e^+ e^-) = 4.229 \times 10^{-6}$  when including all DE and INT terms. The obtained value is compatible with both predictions within the experimental errors. However it should be noted that none of the above predictions includes any radiative or isospin breaking effects.

## 5. Kinematic space study

The current data statistics does not allow a precise enough measurement to quantify the contribution of the DE magnetic term M to the total decay rate (expected to be about 1%). However, the authors of [3,6] have pointed out that the contributions of IB, magnetic M, and interference IB-E terms have different distributions in the Dalitz plot ( $T_\pi^*$ ,  $E_\gamma^*$ ) for different ranges of  $q^2$  values, where  $T_\pi^*$ ,  $E_\gamma^*$  and  $q^2$  are the charged pion kinetic energy and the virtual photon energy in the kaon rest frame, and the  $e^+e^-$  mass squared, respectively. The differences remain relevant even after the analysis selection acceptance is applied. A method based on

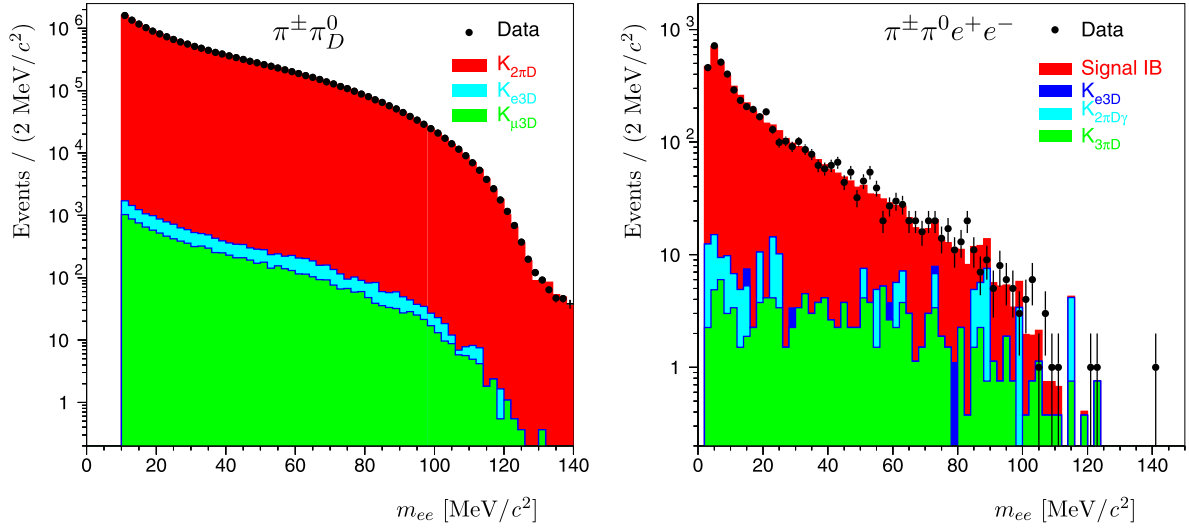


**Fig. 4.** Reconstructed  $e^+e^-$  mass distribution for the normalization (left) and signal (right) candidates with the lower cuts of 10 and 3 MeV/ $c^2$ , respectively. Simulated background and normalization (signal) contributions are also displayed.

the population of 3d-boxes in the kinematic space ( $q^2$ ,  $T_\pi^*$ ,  $E_\gamma^*$ ) is used to determine the relative fraction of each component that would add up to reproduce the data sample population. The data 3d-space is first split into  $N_1$  slices along  $q^2$ , then each slice is split into  $N_2$  slices along  $T_\pi^*$  and then into  $N_3$   $E_\gamma^*$  slices, all with equal populations. The result is a grid of  $N_1 \times N_2 \times N_3$  exclusive 3d-boxes of variable size but identical population. The background contributions and the various simulated signal components are distributed according to the data grid definition, each resulting in a set of 3d-boxes of unequal population. To account for the potentially different sizes of the simulation samples, scale factors  $\rho_M$  and  $\rho_{IB-E}$  are defined as the ratios of the IB to the M and IB to the IB-E simulated sample sizes.

To obtain the fractions (M)/IB and (IB-E)/IB reproducing the data, a  $\chi^2$  estimator is minimized:

$$\chi^2 = \sum_{i=1}^{N_1 \times N_2 \times N_3} (N_i - M_i)^2 / (\delta N_i^2 + \delta M_i^2), \quad (10)$$

where  $N_i$  ( $\delta N_i$ ) is the data population (error) and  $M_i$  ( $\delta M_i$ ) the expected population (error) in box  $i$ . The denominator of each term is dominated by the number of data events  $\delta N_i^2 = N_i$ , the same in each box. The expected number of events in box  $i$  is computed as:

$$M_i = N \times (N_i^{IB} + a \cdot N_i^M + b \cdot N_i^{IB-E}) + N_i^{Bkg}, \quad (11)$$

where  $N$  is a global scale factor to guarantee that the sum of the simulated events and background contributions is normalized to the total number of data candidates. At the end of the minimization, the obtained values of  $a$  and  $b$  can be related to the relative contributions (M)/IB and (IB-E)/IB by:

$$(M)/IB = (a \pm \delta a) / \rho_M, \quad (IB-E)/IB = (b \pm \delta b) / \rho_{IB-E}. \quad (12)$$

The method has no sizeable dependence on the precise grid structure as long as the granularity ensures sensitivity to the population variation within the resolution (at least 3  $q^2$  slices and 5 or 6 slices along the two other variables) and large enough statistics per box to consider Gaussian errors. The grid configuration  $3 \times 5 \times 6$  has been employed and the results are obtained with a  $\chi^2$  probability of 19% for a value of 98.2/87 degrees of freedom and a correlation  $C(a, b) = 0.06$ . The obtained value (M)/IB =  $0.0114 \pm 0.0043_{stat}$  is consistent with the predicted value from

[3],  $1/71 = 0.0141 \pm 0.0014_{ext}$ , obtained using the experimental measurement of  $N_M^{(0)}$ . The (IB-E)/IB value of  $-0.0014 \pm 0.0036_{stat}$  shows that there is no sensitivity to this contribution within the current data statistics and agrees with the value from [6],  $-1/253 = -0.0039 \pm 0.0028_{ext}$ , obtained using experimental inputs to  $N_E^{(0,1,2)}$  values. The external errors on the predicted values stem from the uncertainties of the measurements used as input in the evaluations.

## 6. Asymmetry investigations

Electroweak (or beyond Standard Model) phases change sign under charge conjugation when switching from  $K^+$  to  $K^-$ , unlike the strong phase  $\delta = \delta_0^2 - \delta_1^1$  that governs the final state interaction of the pion system. These phases can be investigated through asymmetries between  $K^+$  and  $K^-$  partial rates.

The simplest CP-violating asymmetry is the charge asymmetry between  $K^+$  and  $K^-$  partial rates integrated over the whole phase space:

$$A_{CP} = \frac{\Gamma(K^+ \rightarrow \pi^+ \pi^0 e^+ e^-) - \Gamma(K^- \rightarrow \pi^- \pi^0 e^+ e^-)}{\Gamma(K^+ \rightarrow \pi^+ \pi^0 e^+ e^-) + \Gamma(K^- \rightarrow \pi^- \pi^0 e^+ e^-)}. \quad (13)$$

The value of  $A_{CP}$  can be related to the interference IB-E term and is proportional to  $\sin \delta \sin \Phi_E$ , where  $\Phi_E$  is a possible CP-violating phase appearing in the form factors  $F_1^{DE}$ ,  $F_2^{DE}$  in addition (subtraction) to the strong phase  $\delta_1^1$  (Section 1). The asymmetry is obtained from the statistically independent measurements of  $K^+$  and  $K^-$  branching ratios, that take into account the possible biases introduced by the detector acceptances. The values

$$\begin{aligned} BR(K^+) &= (4.151 \pm 0.078_{stat}) \times 10^{-6}, \\ BR(K^-) &= (4.394 \pm 0.108_{stat}) \times 10^{-6} \end{aligned} \quad (14)$$

lead to  $A_{CP} = -0.0284 \pm 0.0155$ , where the error is statistical only, as the systematic and external errors cancel in the ratio. This value is consistent with zero and is translated to a single-sided limit:

$$|A_{CP}| < 4.82 \times 10^{-2} \text{ at } 90\% \text{ CL}. \quad (15)$$



Other asymmetries are defined in [3] using the so-called Cabibbo-Maksymowicz [15] variables<sup>34</sup> to describe the kinematic space of the decay and selecting particular integration regions of the  $\phi$  angular variable:

$$A_{CP}^{\phi*} = \frac{\int_0^{2\pi} \frac{d\Gamma_{(K^+-K^-)}}{d\phi} d\phi^*}{\int_0^{2\pi} \frac{d\Gamma_{(K^++K^-)}}{d\phi} d\phi}, \text{ where} \quad (16)$$

$$\int_0^{2\pi} d\phi^* \equiv \left[ \int_0^{\pi/2} - \int_{\pi/2}^{\pi} + \int_{\pi}^{3\pi/2} - \int_{3\pi/2}^{2\pi} \right] d\phi,$$

$$A_{CP}^{\tilde{\phi}} = \frac{\int_0^{2\pi} \frac{d\Gamma_{(K^+-K^-)}}{d\phi} d\tilde{\phi}}{\int_0^{2\pi} \frac{d\Gamma_{(K^++K^-)}}{d\phi} d\phi}, \text{ where} \quad (17)$$

$$\int_0^{2\pi} d\tilde{\phi} \equiv \left[ \int_0^{\pi/2} + \int_{\pi/2}^{\pi} - \int_{\pi}^{3\pi/2} - \int_{3\pi/2}^{2\pi} \right] d\phi.$$

These asymmetries can be obtained by combining the branching ratios measured in various parts of the  $\phi$  variable space. Defining sectors of the  $\phi$  space between 0 and  $2\pi$  as  $\Phi 1$  ( $0, \pi/2$ ),  $\Phi 2$  ( $\pi/2, \pi$ ),  $\Phi 3$  ( $\pi, 3\pi/2$ ) and  $\Phi 4$  ( $3\pi/2, 2\pi$ ), and combining them as statistically independent sector sums ( $\Phi 13 = \Phi 1 + \Phi 3$ ,  $\Phi 24 = \Phi 2 + \Phi 4$ ) and ( $\Phi 12 = \Phi 1 + \Phi 2$ ,  $\Phi 34 = \Phi 3 + \Phi 4$ ) one can obtain the above asymmetries.

The  $\phi^*$  integral has the interesting property of subtracting the contribution of sector sum  $\Phi 24$  from the contribution of sector sum  $\Phi 13$ . The interference term IB-M (Section 1) equally populates sectors  $\Phi 1$  and  $\Phi 3$  when positive and depopulates sectors  $\Phi 2$  and  $\Phi 4$  when negative. The  $A_{CP}^{\phi*}$  asymmetry is then related to the interference IB-M term and is proportional to  $\cos \delta \sin \Phi_M$ , where  $\Phi_M$  is a possible CP-violating phase appearing in the form factor  $F_3^{DE}$  (Section 1). The interference IB-M term has not been generated in the simulation as it is not expected to contribute significantly to the total rate. However it has been checked that the whole range of the  $\phi$  variable is always considered in the acceptance calculation, apart for the region  $q^2 < 3$  (MeV/c<sup>2</sup>)<sup>2</sup> excluded from the signal selection. The CP asymmetries defined in Eq. (16, 17) are measured, although to a limited precision given the current data statistics, as:

$$A_{CP}^{\phi*} = 0.0119 \pm 0.0150_{\text{stat}} \quad \text{and} \quad A_{CP}^{\tilde{\phi}} = 0.0058 \pm 0.0150_{\text{stat}}. \quad (18)$$

All asymmetries are consistent with zero, single-sided upper limits can be set as

$$|A_{CP}^{\phi*}| < 3.11 \times 10^{-2}, |A_{CP}^{\tilde{\phi}}| < 2.50 \times 10^{-2} \text{ at } 90\% \text{ CL}. \quad (19)$$

<sup>34</sup> For  $K^\pm$  decays, the variables are the squared invariant dipion and dilepton masses, the angle of the  $\pi^\pm$  ( $e^\pm$ ) in the dipion (dilepton) rest frame with respect to the flight direction of the dipion (dilepton) in the  $K^\pm$  rest frame, the angle  $\phi$  between the dipion and dilepton planes in the kaon rest frame.

Following another prescription of [3], a long-distance P-violating asymmetry defined as

$$A_P^{(L)} = \frac{\int_0^{2\pi} \frac{d\Gamma}{d\phi} d\phi^*}{\int_0^{2\pi} \frac{d\Gamma}{d\phi} d\phi} = \frac{\Gamma(\Phi 13) - \Gamma(\Phi 24)}{\Gamma} \quad (20)$$

can be obtained from the asymmetry between sector sums  $\Phi 13$  and  $\Phi 24$  when considering  $K^+$  or  $K^-$  alone, and combined if found consistent. The  $A_P^{(L)}$  asymmetry is proportional to  $N_M^{(0)}$  [3] and  $\sin \delta$ . A precise  $A_P^{(L)}$  measurement would allow a check of the sign of  $N_M^{(0)}$  and a measurement of  $\sin \delta$ .

Our data lead to  $A_P^{(L)}(K^+) = 0.0059 \pm 0.0180_{\text{stat}}$  and  $A_P^{(L)}(K^-) = -0.0166 \pm 0.0237_{\text{stat}}$ , both consistent with zero. The combined value is  $A_P^{(L)}(K^\pm) = -0.0023 \pm 0.0144_{\text{stat}}$ . The errors are statistical only as both systematic and external uncertainties cancel in the ratios. This value can be translated into a single-sided upper limit:

$$|A_P^{(L)}| < 2.07 \times 10^{-2} \text{ at } 90\% \text{ CL}. \quad (21)$$

## 7. Results and conclusion

The data sample recorded by the NA48/2 experiment in 2003–2004 has been analyzed, searching for the unobserved  $K^\pm \rightarrow \pi^\pm \pi^0 e^+ e^-$  decay mode in an exposure of  $1.7 \times 10^{11}$  kaon decays. A sample of 4919 decay candidates with 4.9% background has been identified, resulting in the first observation of this decay mode. The branching ratio has been measured relative to the  $K^\pm \rightarrow \pi^\pm \pi^0$  mode followed by a Dalitz decay  $\pi_D^0 \rightarrow e^+ e^- \gamma$  and found to be  $(4.237 \pm 0.063_{\text{stat}} \pm 0.033_{\text{syst}} \pm 0.126_{\text{ext}}) \times 10^{-6}$ , in agreement with predictions from ChPT.

Despite the limited statistics available, a study of the kinematic space of the decay has been performed to extract information on the fraction of magnetic (M) and interference (IB-E) contributions with respect to inner bremsstrahlung (IB). The relative contribution, (M)/IB =  $(1.14 \pm 0.43_{\text{stat}}) \times 10^{-2}$ , is found consistent with the theoretical expectation of  $(1.41 \pm 0.14_{\text{ext}}) \times 10^{-2}$ . The relative IB-E contribution, (IB-E)/IB =  $(-0.14 \pm 0.36_{\text{stat}}) \times 10^{-2}$ , is also in agreement with the prediction of  $(-0.39 \pm 0.28_{\text{ext}}) \times 10^{-2}$  but with limited significance due to the lack of data statistics in the high  $m_{ee}$  region.

Several CP-violating asymmetries and a long-distance P-violating asymmetry have been evaluated and found to be consistent with zero, leading to upper limits  $|A_{CP}| < 4.8 \times 10^{-2}$ ,  $|A_{CP}^{\phi*}| < 3.1 \times 10^{-2}$ ,  $|A_{CP}^{\tilde{\phi}}| < 2.5 \times 10^{-2}$ ,  $|A_P^{(L)}| < 2.1 \times 10^{-2}$  at 90% CL.

If larger data statistics becomes available (for example at the NA62 experiment), more detailed studies of the kinematic space will allow for an improved evaluation of the DE term contribution. A study of the P-violating asymmetry could bring information on the sign of the DE magnetic term and on the strong phase  $\delta$  involved in the final state interaction of the two pions.

## Acknowledgements

We gratefully acknowledge the CERN SPS accelerator and beam line staff for the excellent performance of the beam and the technical staff of the participating institutes for their efforts in the maintenance and operation of the detector, and data processing. We thank M. Koval for making the “Prague” radiative  $\pi^0$  Dalitz

decay code available in the NA48/2 simulation software. Discussions with G. D'Ambrosio and O. Catà were most stimulating in clarifying the impact of interference terms on our measurement.

## References

- [1] V. Cirigliano, G. Ecker, H. Neufeld, A. Pich, J. Portolés, *Rev. Mod. Phys.* **84** (2012) 399.
- [2] H. Pichl, *Eur. Phys. J. C* **20** (2001) 371.
- [3] L. Cappiello, O. Catà, G. D'Ambrosio, D.N. Gao, *Eur. Phys. J. C* **72** (2012) 1872.
- [4] S.R. Gevorkyan, M.H. Misheva, *Eur. Phys. J. C* **74** (2014) 2860.
- [5] J.R. Batley, et al., NA48/2 Collaboration, *Eur. Phys. J. C* **68** (2010) 75.
- [6] L. Cappiello, O. Catà, G. D'Ambrosio, *Eur. Phys. J. C* **78** (2018) 265.
- [7] J.R. Batley, et al., NA48/2 Collaboration, *Eur. Phys. J. C* **52** (2007) 875.
- [8] V. Fanti, et al., NA48 Collaboration, *Nucl. Instrum. Methods A* **574** (2007) 443.
- [9] M. Tanabashi, et al., Particle Data Group, *Phys. Rev. D* **98** (2018) 030001.
- [10] GEANT3 Detector Description & Simulation Tool, CERN Program Library W5013 (1994).
- [11] C. Gatti, *Eur. Phys. J. C* **45** (2006) 417.
- [12] T. Husek, K. Kampf, J. Novotný, *Phys. Rev. D* **92** (2015) 054027.
- [13] E. Barberio, Z. Wąs, *Comput. Phys. Commun.* **79** (1994) 291.
- [14] Qingjun Xu, Z. Wąs, in: RADCOR2009, PoS 071 (2009).
- [15] N. Cabibbo, A. Maksymowicz, *Phys. Rev.* **137** (1965) B438.